

Generation of an internal tide by surface tide/eddy resonant interactions

M.-P. Lelong and E. Kunze

Abstract The interaction of surface tidal currents and baroclinic geostrophic eddies is considered to determine whether energy can be transferred to baroclinic tides by this process. Theoretical and numerical analyses reveals that when the surface tide is uniform in the horizontal, the interaction is identically zero, even under resonant conditions. The resonant interaction results in maximum internal wave excitation when the horizontal scale of the tide is comparable to that of the eddies. Thus, this process is not an efficient mechanism for internal wave excitation in the deep ocean where barotropic tides vary over much larger scales than the eddies, but it may provide an additional wave source at low latitudes and in coastal regions where tidal horizontal modulation by topography can be significant.

1 Introduction

A series of surface-drifter observations in the western boundary current of the subpolar North Pacific found intense near-inertial/near-diurnal frequency motions trapped within anticyclonic warm-core rings (Rogachev *et al.*, 1992; Rogachev *et al.*, 1996; Rogachev and Carmack, 2002). The authors speculated that the lower bound of the internal wave frequency band had been locally decreased by the rings' negative vorticity (Kunze, 1985), thereby trapping near-inertial waves within the rings. The proximity of near-inertial and near-diurnal frequencies led them to conjecture that the observed waves might have resulted from a diurnal-tide/eddy interaction. However, given their limited data, they could not rule out the role of wind-forcing or subinertial instability, and the evidence for the suspected role of

M.-Pascale Lelong
NorthWest Research Associates, P.O. Box 3027 Bellevue WA 98009-3027, e-mail: pascale@nwra.com

Eric Kunze
University of Victoria, e-mail: kunze@uvic.ca

the barotropic tide was circumstantial. Nor was the interpretation of these observations substantiated by any rigorous theoretical arguments.

Research into tidal generation of linear internal waves in the deep ocean has largely focused on the interaction of surface tidal currents with topography (e.g. Cox and Sandstrom, 1962; Wunsch, 1975; Simmons *et al.*, 2004; Garrett and Kunze, 2007), but the mechanism of tide/eddy interaction has not, to our knowledge, been previously considered. The objective of our combined theoretical and numerical study is to assess conditions under which internal waves can be generated following interaction of an oscillating tidal current with a baroclinic geostrophic eddy field.

A summary of the weakly nonlinear theory, first presented in Lelong and Kunze (2009), is given in Section 2. Numerical results are presented in section 3. Section 4 includes a discussion of results and concluding remarks.

2 Problem definition

This section provides a mathematical description of the problem. Equations of motion are given in Sec. 2.1. The analogy between resonant wave triads and tide/eddy interactions is explained in Sec. 2.2, followed by a summary of the multiple-scale analysis in Sec. 2.3.

2.1 Governing equations

Because of their barotropic structure, tidal flow studies are typically formulated with the rotating shallow-water equations. Here, the focus on internal wave generation and the baroclinicity of the eddy field suggests instead that we use a 3D Boussinesq model with f -plane rotation,

$$\frac{\partial \mathbf{u}_h}{\partial t} + (\mathbf{u}_h \cdot \nabla_h) \mathbf{u}_h + w \frac{\partial \mathbf{u}_h}{\partial z} + \nabla_h p + f \hat{e}_3 \times \mathbf{u}_h = \hat{e}_1 F(x, y, t) \quad (1a)$$

$$\frac{\partial w}{\partial t} + (\mathbf{u}_h \cdot \nabla_h) w + w \frac{\partial w}{\partial z} + \frac{\partial p}{\partial z} - b = 0 \quad (1b)$$

$$\frac{\partial b}{\partial t} + (\mathbf{u}_h \cdot \nabla_h) b + w \frac{\partial b}{\partial z} + N^2 w = 0 \quad (1c)$$

$$\nabla_h \cdot \mathbf{u}_h + \frac{\partial w}{\partial z} = 0, \quad (1d)$$

where $\mathbf{u}_h = \{u, v\}$ is the horizontal velocity, w the vertical velocity, $b = -g\rho/\rho_0$ the buoyancy and p the pressure. f is the Coriolis frequency and $N = \sqrt{-\frac{g}{\rho_0} \frac{d\rho(z)}{dz}}$ the

constant buoyancy frequency, defined in terms of the mean density profile $\overline{\rho(z)}$. \hat{e}_1 and \hat{e}_3 are unit vectors in the x and z directions.

The effect of the barotropic tide is incorporated as a time-dependent forcing term

$$F(x, y, t) = U(x, y) \frac{\omega_1^2 - f^2}{\omega_1} \cos \omega_1 t$$

on the right-hand-side of the x -momentum equation. This forcing represents a parameterization of the variation of sea-surface slope with the tidal cycle and is chosen to elicit a response of the form $u = U(x, y) \sin \omega_1 t$ where ω_1 denotes the tidal frequency. In the following analysis, we will assume that U is a function of y only, $U = U(y)$.

The eddy field, consisting of an array of 3D Taylor-Green vortices, is introduced as an initial condition in geostrophic and hydrostatic balance,

$$u(t=0) = U_e(t=0) \cos k_2 x \sin l_2 y \cos m_2 z \quad (2a)$$

$$v(t=0) = - \int \frac{\partial u}{\partial x} \Big|_{t=0} dy \quad (2b)$$

$$w(t=0) = 0 \quad (2c)$$

$$b(t=0) = \int \frac{\partial v}{\partial z} \Big|_{t=0} dx \quad (2d)$$

$$p(t=0) = \int v(t=0) dx. \quad (2e)$$

2.2 Wave-triad interactions

The interaction between a barotropic tide and an eddy field bears similarities with internal wave-triad interactions where the resonant interaction of two waves leads to the excitation of a third (McComas and Bretherton, 1977; Müller *et al.*, 1986), and with the resonant interaction between wind-forced pure inertial oscillations and a turbulent mesoscale eddy field that results in the excitation of a propagating near-inertial internal wave (Danioux and Klein, 2008).

To illustrate the analogy, we consider a barotropic semidiurnal tide with wavevector $\kappa_1 = \{0, l_1, 0\}$ and frequency ω_1 in the presence of an eddy field characterized by wavevector $\kappa_2 = \{k_2, l_2, m_2\}$ and advective time-scale $1/(\kappa_2 \cdot U_e) \gg 2\pi/\omega_1$ where U_e is a typical eddy velocity. The nonlinear quadratic interaction of the tide with the eddies excites motions with functional form

$$e^{i[k_2 x \pm (l_1 \pm l_2)y \pm m_2 z \pm \omega_1 t]}.$$

As in the wave-wave interaction problem, the resulting signal is weak under most conditions. However, if the scales of the barotropic tide and eddy field are such that

resonance conditions,

$$\kappa_1 \pm \kappa_2 = \kappa_3 \quad (3a)$$

$$\omega_1 = \omega(\kappa_1 \pm \kappa_2). \quad (3b)$$

where ω is the internal wave dispersion relation

$$\omega(\kappa_3) = \sqrt{\frac{N^2(k_3^2 + l_3^2) + f^2 m_3^2}{k_3^2 + l_3^2 + m_3^2}}, \quad (4)$$

then resonance conditions are satisfied and stronger interaction possible, exciting an inertia-gravity wave (IGW) whose frequency ω_3 matches that of the tide ω_1 and wavevector $\kappa_3 = \{k_3, l_3, m_3\} = \{k_2, l_1 + l_2, m_2\}$. In this case, the resonant triad is comprised of the barotropic tide, eddy field and IGW components with characteristic scales given above.

2.3 Multiple-scale analysis

The interaction has been examined with a weakly nonlinear multiple-scale perturbation method based on a fast wavelike timescale $T_0 \sim 1/f$, and a much longer, advective eddy timescale $T_1 \sim U_e/L$ where L is a typical eddy radius (Lelong and Kunze, 2009). The ratio of the two timescales defines a small parameter, $U/fL = \varepsilon$, known as the Rossby number. In the usual fashion, all variables are expressed as power series expansions in ε (Kevorkian and Cole, 1981), e.g. for velocity,

$$\mathbf{u}(\mathbf{x}; t_0, t_1) = \mathbf{u}^{(0)}(\mathbf{x}; t_0, t_1) + \varepsilon \mathbf{u}^{(1)}(\mathbf{x}; t_0, t_1) + O(\varepsilon^2)$$

where t_0 and t_1 denote nondimensionalized fast and slow times respectively such that $\partial/\partial t = \partial/\partial t_0 + \varepsilon \partial/\partial t_1$.

The next step consists in delineating the triad components. To lowest order in ε , we assume that both tide and eddy velocities are entirely horizontal.

The barotropic tide velocity is defined to be the vertically averaged horizontal velocity over the domain depth H

$$\mathbf{u}_{BT} = \overline{\mathbf{u}_h(\mathbf{x}; t_0, t_1)} = \frac{1}{H} \int_0^H \mathbf{u}_h(\mathbf{x}; t_0, t_1) dz. \quad (5)$$

The tide oscillates on the fast timescale but its amplitude may be modulated on the slower timescale. Tidal equations are obtained by vertically averaging Eqs. 1a-d.

The eddy velocity is independent of the fast timescale and defined as the temporally averaged horizontal velocity

$$\mathbf{u}_e(\mathbf{x}, t_1) = \overline{\mathbf{u}_h(\mathbf{x}; t_0, t_1)} = \frac{1}{\tau} \int_{t_0}^{t_0+\tau} \mathbf{u}_h(\mathbf{x}; \tau_0, t_1) d\tau_0 \quad (6)$$

where $T_0 \ll \tau \ll T_1$. Eddy field equations are obtained by temporally averaging Eqs. 1a-d.

The residual horizontal velocity which is ascribed to internal waves possesses vertical structure and is a function of both timescales. To lowest order, the vertical velocity is also assigned to the wave component,

$$\mathbf{u}_{wave} = \{\mathbf{u}_h - \mathbf{u}_{BT} - \mathbf{u}_e, w\}. \quad (7)$$

The internal wave evolution is best described by a forced wave equation, derived from Eqs. 1a-d through algebraic manipulation. In nondimensional form, it is

$$\varepsilon^2 \frac{\partial^2}{\partial t_0^2} \nabla_h^2 w + \frac{\partial^2}{\partial t_0^2} \left(\frac{\partial^2 w}{\partial z^2} \right) + \nabla_h^2 w + \frac{\partial^2 w}{\partial z^2} = \varepsilon(F_1 + F_2 + F_3 + F_4 + F_5) + \varepsilon^3 F_6 \quad (8)$$

where the right-hand-side forcing terms

$$F_1 = \frac{\partial^2}{\partial t \partial z} \nabla_h \cdot [(\mathbf{u}_h \cdot \nabla_h) \mathbf{u}_h] \quad (9a)$$

$$F_2 = \frac{\partial^2}{\partial t \partial z} \nabla_h \cdot \left[w \frac{\partial \mathbf{u}_h}{\partial z} \right] \quad (9b)$$

$$F_3 = -\nabla_h^2 [\mathbf{u}_h \cdot \nabla_h b] \quad (9c)$$

$$F_4 = -\nabla_h^2 \left[w \frac{\partial b}{\partial z} \right] \quad (9d)$$

$$F_5 = \frac{\partial}{\partial z} \{ \mathbf{e}_3 \cdot [\nabla \times (\mathbf{u} \cdot \nabla) \mathbf{u}_h] \} \quad (9e)$$

$$F_6 = -\frac{\partial}{\partial t} \nabla_h^2 [\mathbf{u}_h \cdot \nabla_h w]. \quad (9f)$$

There are no non-trivial solutions to Eq. 8 at $O(1)$ and $O(\varepsilon)$. At $O(\varepsilon^2)$, the forcing terms each contain contributions from eddy/eddy, tide/eddy and tide/tide interactions. Homogeneous solutions of Eq. 8 are of the form $\exp[\pm i(kx + ly + mz \pm \omega t)]$ where $\omega^2 = 1 + (k^2 + l^2)/m^2$ is the nondimensional form of Eq. 4 when $m > \sqrt{k^2 + l^2}$. When forcing terms satisfy the homogeneous equation, resonance occurs, similar to the resonant response of a harmonic oscillator forced at its natural frequency. Not all solutions of Eq. 8 represent propagating IGWs, but our present focus is on forced solutions that exhibit propagating internal-wave $\exp[\pm i(k_2 x + (l_1 \pm l_2)y + m_2 z \pm \omega_1 t)]$ behaviour described in Sec. 2.2. Resonant solutions can only be excited if the F_i terms project onto matching frequency and wavenumber ranges (Ford *et al.*, 2000). This implies that eddy/eddy interactions,

which occur on very long time-scales, cannot excite an internal tide since their projection onto the IGW-frequency band is zero. Similarly, tide/tide interactions cannot project onto IGW vertical scales. Therefore, we need only consider tide/eddy contributions and, more specifically, ones that trigger a resonant response, of the form $\sin \theta$ and $\cos \theta$ where

$$\theta = k_2 x \pm (l_1 + l_2)y \pm m_2 z - \omega_1 t_0 = k_3 x \pm l_3 y \pm m_3 z \pm \omega_3 t_0.$$

Coefficients for sine and cosine terms are

$$C_s^\pm(t_1) = u_e^{(0)}(t_1) u_{BT}^{(0)}(t_1) \frac{k_2 l_1 m_2}{4} (\pm 1 \pm \frac{3l_1}{4l_2}) \quad (10)$$

$$C_c^\pm(t_1) = u_e^{(0)}(t_1) u_{BT}^{(0)}(t_1) \frac{l_1 m_2}{16\omega_1} (\mp l_1 \pm \frac{k_2^2}{l_2} \mp l_2 \pm \frac{2k_2^2 \omega_1^2}{l_2}). \quad (11)$$

For circularly shaped eddies ($k_2 = l_2$), C_s^\pm and C_c^\pm achieve a maximum when $l_1 = -\frac{2}{3}l_2$ and $l_1 = -\frac{4}{3}l_2$ respectively. This yields $l_3 = \pm \frac{l_2}{3}$, which implies that l_1/l_2 must be $O(1)$ for resonant forcing to be most effective.

When barotropic tidal wavenumber $l_1 = 0$, $F_1^{(0)} \equiv 0$ since $\nabla_h \cdot \mathbf{u}_e^{(0)} = 0$. Moreover, the sum of $F_3^{(0)}$ and $F_5^{(0)}$ exactly cancels due to thermal-wind balance since $F_3^{(0)} = -\nabla_h^2 [u^{(0)} \frac{\partial b^{(0)}}{\partial x}]$ and $F_5^{(0)} = \frac{\partial^2}{\partial z \partial x} [(\mathbf{u}^{(0)} \cdot \nabla)v^{(0)}] = \frac{\partial^2}{\partial z \partial x} [u^{(0)} \frac{\partial v^{(0)}}{\partial x}]$. Therefore, if the barotropic tide velocity is uniform, no waves can be excited since all tide/eddy forcing terms vanish. This result is independent of whether resonance conditions are satisfied or not. Physically, this situation corresponds to a periodic advection of the entire water column by the tidal current. Without any horizontal modulation, this type of motion cannot transfer horizontal energy to vertical motions.

Additional details of the weakly nonlinear solutions are given in Lelong and Kunze (2009).

3 Numerical simulations

Numerical simulations were performed to check the weakly nonlinear theory. The numerical model solves the three-dimensional Boussinesq equations on the f -plane (Winters et al., 2004) in a domain of dimension $L_x \times L_y \times L_z$. Boundary conditions are periodic in both horizontal directions and free-slip in the vertical. To assess the role of the barotropic tide, we compare the evolution of two different simulations (Runs A and B) that differ only in their tidal forcing. In both cases, the initial condition consists of a field of vortices in geostrophic and hydrostatic equilibrium, modulated by Gaussian (in x) and exponential (in z) envelope functions to confine the eddy field to upper and middle regions of the domain. This configuration allows

generated waves to radiate away from the presumed eddy source region. The initial vorticity distribution for Run B is shown in Fig. 1.

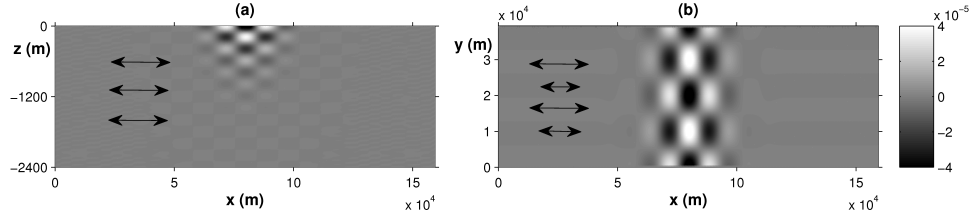


Fig. 1 vertical (a) and horizontal (b) cross-sections of vorticity field at $t = 0$ for Run B. Arrows indicate the direction and spatial variation of the barotropic tidal forcing.

Tidal forcing is ramped up to full strength over five tidal cycles to ensure smoothness of solutions. Principal run parameters are given in Table 1. Coriolis and buoy-

Table 1 Simulation parameters for domain size $L_x \times L_y \times L_z$, tidal wavelength λ_1 and eddy wavelength λ_2 .

Run	Tide	L_y	L_x	L_z	λ_1	λ_2
A	$0.03m s^{-1}$	$6.25 \times 10^4 m$	$2.5 \times 10^5 m$	$2400m$	∞	$3.12 \times 10^4 m$
B	$0.03m s^{-1}$	$4 \times 10^4 m$	$1.6 \times 10^5 m$	$2400m$	$1.33 \times 10^4 m$	$2 \times 10^4 m$

ancy frequencies are $f = 10^{-4} s^{-1}$ and $N = 5 \times 10^{-3} s^{-1}$ respectively. This yields $N/f = 50$, somewhat smaller than typical oceanic values. Using a reduced value of N/f while simultaneously reducing horizontal scales of eddies and tide preserves dynamical similarity with oceanographically relevant parameter regimes in situations such as this one where the large range of spatial and temporal scales that must be resolved becomes prohibitively expensive (e.g. Lelong and Sundermeyer, 2005).

Runs A and B differ in the horizontal scale, $\lambda_1 = 2\pi/l_1$, of the tidal forcing. In Run A, λ_1 is much larger than the scale of the dominant eddies $\lambda_2 = 2\pi/l_2$, a case characteristic of deep-ocean conditions. In contrast, in Run B, $\lambda_1 = O(\lambda_2)$, as might occur on the continental shelf or at low latitudes. In both Runs B and C, eddy and tide parameters are chosen to satisfy resonance conditions Eqs. 3a,b.

All runs, including one in which the tide was turned off (not shown), exhibit some degree of low-level internal wave radiation initially. Some weak radiation occurs because the balance of the initial flow is inherently limited by finite numerical resolution. This was confirmed by noting a decrease in initial wave radiation with increasing numerical resolution (not shown). Another source of waves arises from the initial array of localized vortices not being an exact solution of the nonlinear

equations (in contrast to the periodic array of vortices used in Sec. 2.3). Over time, nonlinear effects act to distort the initial state, resulting in some wave radiation. This was verified numerically by performing a linear simulation in which nonlinear terms and tidal forcing were set to zero. In this case (not shown), the vortices retained their initial balanced state and the resulting wave radiation dropped by several orders of magnitude compared to the nonlinear case.

In Run B, eddy and tidal scales are chosen to maximize the strength of the forcing terms in Eq. 10. L_y encompasses exactly two λ_2 and three λ_1 . To allow for horizontal and vertical wave propagation, $L_x = 4L_y$, and in the vertical $L_z = 6\lambda_{z_2}$ where $\lambda_{z_2} = 2\pi/m_2$.

If residual u and v (defined by Eq. 7) and w represent linear internal waves of frequency ω_1 and wavevector κ_3 , then u and v components should be $\pi/2$ out of phase and their amplitudes should differ by a factor of ω_1/f . Similarly, w will be π out of phase with residual u and scale as $(\kappa_{h_3}/m_3)u$. Residual u , $(\omega_1/f)v$ and $-(m_3/\kappa_{h_3})w$ are plotted for each simulation in Fig. 3. In Run A, corresponding to the case where $l_1 = 0$ in the theory, residual horizontal velocities are inertial oscillations (Lelong and Kunze, 2009). The residual velocities in Run B, for which resonant forcing is maximum, are an order of magnitude larger than in Run A and have phase behavior consistent with propagating internal waves. The velocities, which are initially zero, begin to grow in response to the strong interaction between tidal and eddy fields. (Fig. 3c). They oscillate with the tidal frequency and their amplitudes grow on the slow time scale.

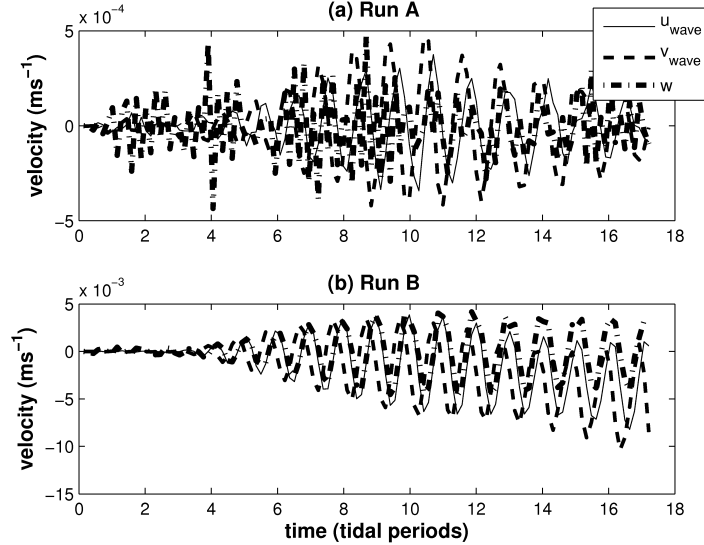


Fig. 2 Time evolution of u , $(\omega_1/f)v$ and $-(m_3/\kappa_{h_3})w$ for Runs A ($\lambda_1 \gg \lambda_2$) and B ($\lambda_1 \approx \lambda_2$), at a point away from the eddy field.

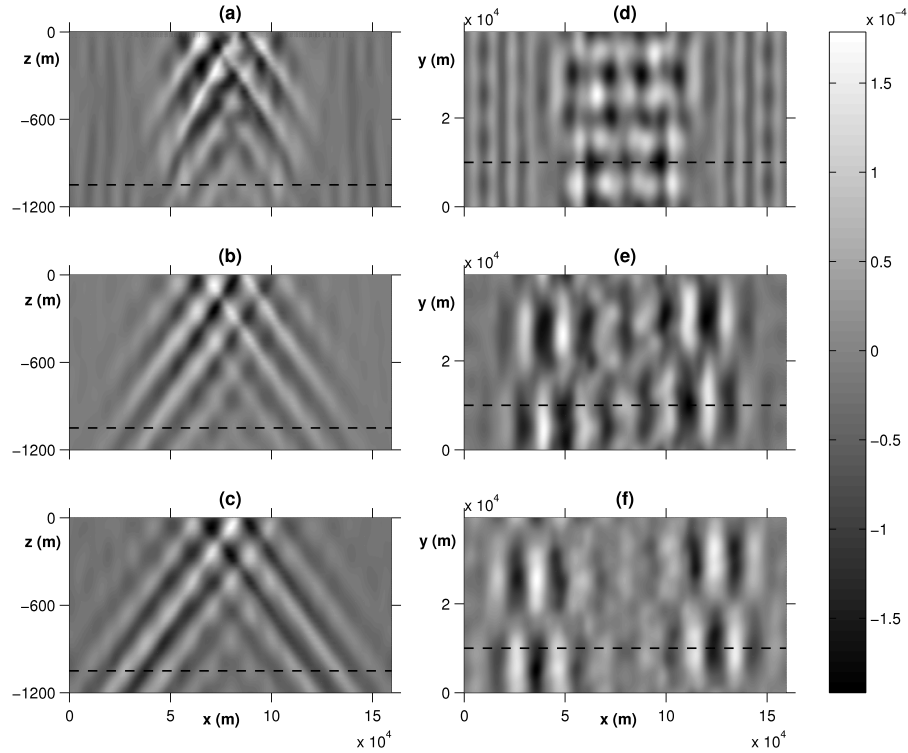


Fig. 3 Cross-sections of w in Run B at $t=3.5 T$ (a,d), $t=7 T$ (b,e) and $10 T$ (c,f); T is the tidal period. Left panels represent vertical cross-sections (only top half of domain is shown), right panels horizontal cross-sections; dotted lines indicate corresponding positions of horizontal and vertical planes. Displayed data spans $\pm 2 \times 10^{-4} m s^{-1}$.

Cross-sections of w at three different times for Run B are shown in Fig. 3. The first emitted waves, visible on the outer edges of Fig. 3 (a,d) are barotropic and lack horizontal structure. These weak waves radiate in response to the initial adjustment discussed above. The next set of emitted waves, visible on the flanks of the eddy region by $t = 3T$ [Fig. 3 (a,d)], are much stronger and exhibit well defined vertical and horizontal structure. By $t = 7T$, definite mode-1 horizontal wavelength in y and mode-6 vertical wavelength are evident (Fig. 3(b,e)), corresponding to $l_3 = l_1 - l_2$ and $m_3 = m_2$, as predicted by the theory for resonantly forced waves. Analysis shows that the energy source for the waves is the eddy field rather than the tide (Lelong and Kunze, 2009). This is quite different from the resonant forcing of internal waves by interaction of near-inertial oscillations and geostrophic eddies (Danioux and Klein, 2008), in which the eddy field acts as a catalyst in transferring near-inertial energy to waves.

4 Conclusions

The interaction of a barotropic tide with a geostrophic eddy field as a potential internal wave source has been examined theoretically and numerically. As predicted by the theory, interaction is negligible when the tidal wavelength is much larger than the eddies' even when resonance conditions are met. When the tide varies on lengthscales comparable to the eddy field's, resonant interaction is maximized. This is unlikely to occur in the mid- and high-latitude open ocean where barotropic tidal lengths are $O(1000 \text{ km})$ while dominant eddy lengthscales are at the Rossby lengthscale $U/f \sim O(100 \text{ km})$. These two lengthscales become more comparable on the continental shelf and at low latitudes. We conclude that the mechanism of eddy/tide interaction, conjectured by Rogachev *et al.* (1992) to explain the intense near-inertial waves observed in western North Pacific anticyclonic vortices, is unlikely. The observed oscillations were more likely wind-generated near-inertial waves.

In the deep ocean, shallow-water waves can exist for $f \ll \omega \ll \sqrt{g/H}$ ($\sim 5 \times 10^{-2} \text{ rad s}^{-1}$ for water depth $H = 400 \text{ m}$) with horizontal wavelengths much greater than H . Though there is little barotropic variance outside of tidal frequencies, higher frequencies with lengthscales matching those of the eddy field will more efficiently transfer energy to internal waves than tidal frequencies (Lelong and Kunze, 2009).

Acknowledgements Support from the Office of Naval Research for the original phase of this study is gratefully acknowledged.

References

1. Bell, T.H., 1975: Topographically generated internal waves in the open ocean. *J. Geophys. Res.*, **80**, 320-327.
2. Cox, C., & H. Sandstrom, 1962: Coupling of internal and surface waves in water of variable depth. *J. Oceanogr. Soc. Japan*, **18**, 499-513.
3. Danioux, E. & P. Klein, 2008: A resonance mechanism leading to wind-forced motions with a $2f$ frequency *J. Phys. Oceanogr.*, submitted.
4. Ford, R., M.E. McIntyre & W.A. Norton, 2000: Balance and the Slow Quasimanifold: Some Explicit Results. *J. Atmos. Sci.*, **57**, 9, 1236-1254.
5. Garrett, C., & E. Kunze, 2007: Internal tide generation in the deep ocean. *Ann. Rev. Fluid Mech.*, **39**, 57-87.
6. Kevorkian, J. & J.D. Cole, 1981: Perturbation methods in applied mathematics. *Applied Mathematical Sciences*, 34, Springer.
7. Kunze, E., 1985: Near-inertial wave propagation in geostrophic shear. *J. Phys. Oceanogr.*, **15**, 544-565.
8. Lelong, M.-P. and E. Kunze, 2009: Can barotropic current/geostrophic eddy interactions excite internal waves?, manuscript in preparation for *J. Fluid Mech.*
9. Lelong, M.-P. and M.A. Sundermeyer, 2005: Geostrophic adjustment of an isolated diapycnal mixing event and its implications for small-scale lateral dispersion. *J. Phys. Oceanogr.*, **35**, 2352-2367.

10. McComas, C.H., & F.P. Bretherton, 1977: Resonant interaction of oceanic internal waves. *J. Geophys. Res.*, **83**, 1397-1412.
11. Müller, P., G. Holloway, F. Henyey & N. Pomphrey, 1986: Nonlinear interactions among internal gravity waves. *Rev. Geophys.*, **24**, 493-536.
12. Rogachev, K.A., E. Carmack, M. Miyaki, R. Thompson & G.I. Yurasov, 1992: Drifting buoy in an anticyclonic eddy of the Oyashio Current. *Doklady Rossiyskoy Akademii Nauk*, **326**, 547-550.
13. Rogachev, K.A., A.S. Salomatina, V.I. Yusupov & E.C. Carmack, 1996: On the internal structure of the Kuril Current anticyclonic eddies. *Okeanologiya*, **36**, 247-354.
14. Rogachev, K.A. & E.C. Carmack, 2002: Evidence for the trapping and amplification of near-inertial motions in a large anticyclonic ring in the Oyashio. *J. Oceanogr.*, **58**, 673-682.
15. Simmons, H.L., R.W. Hallberg & B.K. Arbic, 2004: Internal wave generation in a global baroclinic tidal model. *Deep-Sea Res. II*, **51**, 3043-3068.
16. Winters, K.B., J.A. MacKinnon and B. Mills, 2004: A spectral model for process studies of rotating, density-stratified flows. *J. Atmos. Ocean. Technol.*, **21**, 69-94.
17. Wunsch, C., 1975: Internal tides in the ocean. *Rev. Geophys. Space. Phys.*, **13**, 167-182.